

100-kT Magnetic field generation using paisley targets by femtosecond laser-plasma interactions

M-A.H. Zosa,^{1,2} Y.J. Gu,² and M. Murakami^{2, a)}

¹⁾*Division of Electrical, Electronic and Infocommunications Engineering, Graduate School of Engineering, Osaka University, 2-1 Yamadaoka, Suita, Osaka 565-0871, Japan*

²⁾*Institute of Laser Engineering, Osaka University, 2-6 Yamadaoka, Suita, Osaka 565-0871, Japan*

(Dated: 2 February 2022)

A target using a paisley pattern generates 100-kT-level magnetic fields. Laser irradiation induces local charge separation on the target, which creates surface currents along the concave surface, generating a magnetic field. For a laser intensity of 10^{21}W cm^{-2} , the target generates a 150-kT magnetic field. We developed a simple model to describe the magnetic field as a function of laser intensity and target radius. A double paisley configuration extends the lifetime of the magnetic field to the picosecond scale. The paisley design generates comparable results even if it is simplified. Thus, it is a robust and modular target suitable for magnetic field applications such as 100-kT magnetic field generation and magnetic reconnection.

^{a)}Electronic mail: murakami-m@ile.osaka-u.ac.jp

Modern developments in relativistic femtosecond lasers^{1,2} and microstructure fabrication^{3,4} have expanded the scope of high energy density physics⁵⁻⁷. Recently, studies have utilized these developments to investigate ion acceleration⁸, magnetic field generation⁹, ultra-high density compression^{10,11}, and pair-creation¹². Generating magnetic fields on the 100-kT scale is exciting because it enables the study of fundamental phenomena such as magnetic reconnection¹³⁻¹⁵. Magnetic fields on this scale are observed in the accretion disks of black holes, which makes them valuable for laboratory astrophysics experiments¹⁶.

Irradiating an “escargot” target with a laser is a well-known scheme to produce a strong magnetic field^{17,18}. It has been used in a laboratory experiment as a magnetic field source¹⁶. Microtube implosion (MTI) is another method for magnetic field generation^{19,20}. In MTI, the implosion of the inner layer of a microtube amplifies a seed magnetic field to the megatesla scale, enhancing its strength by a few orders of magnitude²¹.

Although both setups utilize different approaches to generate a magnetic field, an essential factor is the formation of a surface current^{17,20,22}. In this work, we propose a paisley design to generate a magnetic field without a seed magnetic field. Our paisley design is described mathematically by the following function

$$f(k) = \begin{cases} -\frac{R_0}{2} (\exp [4\pi i k - \pi/2] + 1) & k \in (0, \frac{1}{4}) \\ -\frac{R_0}{2} (\exp [4\pi i k - \pi/2] - 1) & k \in (\frac{1}{4}, \frac{1}{2}), \\ R_0 \exp (2\pi i k - \pi/2) & k \in (\frac{1}{2}, 1) \end{cases}, \quad (1)$$

where R_0 is the radius, and $k \in (0, 1)$ is a parametric variable. The x- and y-coordinates are the real and imaginary parts of eq. (1), respectively. Figure 1(a) graphically depicts Eq. (1).

In this design, surface currents produce a magnetic field on the concave side of the target, which makes the magnetic field easily accessible. The open area makes it easier for incoming particles to interact with the magnetic field. Additionally, the accessible location permits two or more targets to be connected in a modular fashion allowing the generated magnetic fields to interact with each other. Thus, it is suitable in experiments requiring the interaction of two or more magnetic field sources. Various arrangements can be used to study magnetic field phenomena such as magnetic reconnection, magnetic mirrors, and other laboratory astrophysics experiments.

To study the magnetic field generation of the paisley design, we used the 2.5D particle-in-cell (PIC) program, EPOCH²³. The laser parameters were $\lambda_L = 800$ nm, $I_L = 1 \times 10^{21}$ W cm⁻²,

and $\tau_L = 100$ fs for the wavelength, peak intensity, and full-width at half-maximum (FWHM), respectively. The simulations used a $30\ \mu\text{m} \times 30\ \mu\text{m}$ box with a cell size of $\frac{\lambda_L}{100}$, 100 pseudo-ions and 200 pseudo-electron per cell, and a laser propagating in the +x direction. The target consisted of fully ionized carbon with a density of $1 \times 10^{23}\ \text{cm}^{-3}$.

The paisley target generates a surface current via local charge separation. The thickness gradient along the tip creates a larger charge separation around the apex upon laser irradiation [Fig. 1(b)]. The laser strips most of the electrons from the thin sections of the paisley target, but it cannot penetrate the thicker areas. Hence, more electrons are ejected close to the apex. This causes the surface electrons to flow towards the apex [Fig. 1(c)]. The curvature of the surface causes a positive (negative) magnetic field to form on its concave (convex) side [Fig. 1(d)]. Although the magnetic field covers only a few square microns, using a larger target will increase its coverage. When using larger targets, materials with low electron densities, such as foam, are preferred because low-density materials have a larger skin depth. The larger skin depth enables the larger target to maintain the charge separation gradient across the tip. Additionally, if the target is rotated 180° about $y = 0$, the polarity of the magnetic fields flips.

To predict magnitude of the magnetic field in kT, we developed a simple analytic model. The magnetic field strength is $B_z \sim j_e R_0$, and the estimated current density, j_e , is $j_e \sim n_{he} c$. The hot-electron density, n_{he} , is related to I_L by $n_{he} = \eta_a I_L / \mathcal{E} c^{24}$. For relativistic electrons, the average kinetic energy, \mathcal{E} , is approximately $3T_e$, where T_e is the electron temperature. If the electron temperature is estimated using the ponderomotive scaling²⁵, the model is reduced to

$$B_z = 30.3 \frac{\eta_a \sqrt{I_{L20}} R_{0\mu\text{m}}}{\lambda_{\mu\text{m}}}, \quad (2)$$

where I_{L20} is the laser intensity normalized to $10^{20}\ \text{W cm}^{-2}$, η_a is the absorption efficiency, $R_{0\mu\text{m}}$ is characteristic radius given by Eq. (1) in μm , and $\lambda_{\mu\text{m}}$ is the laser wavelength in μm . The magnetic field strength scales as $B_z \sim \sqrt{I_L}$, and linearly with R_0 . Figure 2(a) shows that the peak magnetic field increases with the laser intensity. The FWHM for the magnetic field is $\sim 2\tau_L$. Figure 2(b) shows that the PIC simulation results agree well with Eq. (2) for $\eta_a = 0.4$. According to the model, an absorption efficiency of 0.8 or higher is necessary to reach the megatesla scale for $I_L = 10^{22}\ \text{W cm}^{-2}$. However, at this intensity, the model may inaccurate because non-linear effects are no longer negligible.

Comparing Fig. 2(a) with the simulation parameters, the peak magnetic field coincides with the laser maximum. Additionally, the magnetic field sharply drops once the laser stops interacting with the target. This results in a relatively short magnetic field lifetime. However, using two paisley targets prolongs the magnetic field lifetime [Fig. 3(c)]. In this case, the two lasers hit a pair of paisley targets from the +x and -x-direction. The two targets are separated by a gap to minimize the possibility of electrons flowing directly from the body of one target to the tip of the other. The magnetic field generated by the double paisley setup almost completely covers the void [Figs. 3(a) & (b)]. Additionally, the magnetic field is sustained for much longer than the laser pulse duration. As the system evolves, electrons flow towards the center [Fig. 3(d)] and form a partial current loop [Fig. 3(e)]. This loop is stable and extends the magnetic field’s lifetime to the picosecond scale [Fig. 3(f)]. Although the maximum magnetic field strength has a long lifetime, Fig. 3(e) shows that the magnetic field leaks from the confined space. This results in a gradual reduction of the total magnetized area. By 1 ps, the 100-kT region is estimated to be 20% of the area at 400 fs, and the magnetic field is reduced by one order of magnitude by 2 ps. Figure 1(b) shows that a positive patch forms on the concave-side. It is attributed to the imploding ions. The imploded ions attract electrons whose trajectories are bent by the magnetic field generated by the surface current²⁶. The electron gyro motion around the imploded ions works to sustain the magnetic field for a brief period after the laser has disappeared in the single paisley case. For the double paisley targets, the imploded ion region is more pronounced, which helps sustain a partial current loop [Fig. 3(f)]. In addition, two paisley targets form a more confined region, which delays the expansion of the current loop. The electron collision frequency is calculated using a simple formula²². This formula gives the characteristic time scale of the electron collision, ν_e^{-1} , which is several picoseconds long. Thus, dissipation due to Coulomb collisions is negligible for the duration of the magnetic field. For comparison, we also conducted simulations of a 5 μm “escargot” target. It generates a magnetic field of 150 kT with a picosecond lifetime using the same laser parameters.

A drawback of the paisley design is its intricate shape, which is challenging to fabricate. However, a simplified design will yield comparable results. Figure 4(a), shows that a quarter of a rectangular microtube can be used as a simplified paisley target. Although the design differs from the original one, the core concept of utilizing the thickness gradient to guide the surface current remains. Despite a major change in its appearance, the magnetic field

strength produced by the simplified target is comparable to the paisley design [Fig. 4]. However, it has a slightly smaller cross-section, and a shorter lifetime. Although the simplified design might be easier to fabricate, the original paisley structure is still interesting from a theoretical viewpoint.

Due to its small size, the paisley target is prone to pre-expansion when interacting with the laser’s pre-pulse. To approximate this effect, we modified the initial plasma distribution profile of the paisley target. Figure 5 shows the simulation results of a paisley target with a modified initial density profile [Fig. 5(a)]. Although the area of the magnetic field in Fig. 5(b) is smaller than that in Fig. 1(d), the results show that even when the initial distribution is not ideal, it can still produce 100-kT magnetic fields. The potential 3D-effects is another factor to consider for these targets. The influence of 3D effects should be more prominent on the top and bottom (z-axis) ends of the target because the z-axis expansion on the ends alters the electron dynamics close to the ends. This effect can be mitigated by choosing a relatively long or high aspect-ratio target. For experimental verification, the magnetic field strength can be evaluated by measuring the deflection of a passing ion beam¹⁶.

The paisley target is a robust design to generate a magnetic field without a seed. However, further optimization can still be performed to maximize the generated magnetic field. It has potential for multiple applications due to its flexible and modular design. For the double paisley target, its performance is similar to the “escargot” target for both the magnetic field intensity and lifetime. However, the double paisley target requires two lasers, which is less efficient than the “escargot” target. Nevertheless, the paisley target’s advantage lies in its flexibility. Although the current double paisley setup is used to prolong the magnetic field lifetime, flipping one of the paisley targets will result in two magnetic fields with opposing polarities. This configuration is suitable for studying magnetic reconnection. Additionally, different configurations of the paisley targets may be realized to study other magnetic field interactions.

ACKNOWLEDGMENTS

The authors acknowledge Didar Shokov for the fruitful discussions. Computational resources were provided by the Cybermedia Center, Osaka University. This work was supported by the Japan Society for the Promotion of Science (JSPS). PIC simulations

were performed using EPOCH, developed under UK EPSRC (Grant Nos. EP/G054940, EP/G055165, and EP/G056803).

DATA AVAILABILITY

The data that support the findings of this study are available from the corresponding author upon reasonable request.

AUTHOR DECLARATIONS

Conflict of Interest

The authors have no conflicts to disclose.

REFERENCES

- ¹J. W. Yoon, C. Jeon, J. Shin, S. K. Lee, H. W. Lee, I. W. Choi, H. T. Kim, J. H. Sung, and C. H. Nam, “Achieving the laser intensity of 55×10^{22} w/cm² with a wavefront-corrected multi-PW laser,” *Optics Express* **27**, 20412 (2019).
- ²J. W. Yoon, Y. G. Kim, I. W. Choi, J. H. Sung, H. W. Lee, S. K. Lee, and C. H. Nam, “Realization of laser intensity over 10^{23} w/cm²,” *Optica* **8**, 630 (2021).
- ³K. B. Fritzler and V. Y. Prinz, “3d printing methods for micro- and nanostructures,” *Physics-Uspekhi* **62**, 54–69 (2019).
- ⁴S. Fu, Q. Xia, S. Li, G. Ren, F. Chai, C. Wang, and F. Qu, “Shape-controlled synthesis of 3d copper nicotinate hollow microstructures and their catalytic properties,” *RSC Advances* **6**, 18033–18039 (2016).
- ⁵J. Snyder, L. L. Ji, K. M. George, C. Willis, G. E. Cochran, R. L. Daskalova, A. Handler, T. Rubin, P. L. Poole, D. Nasir, A. Zingale, E. Chowdhury, B. F. Shen, and D. W. Schumacher, “Relativistic laser driven electron accelerator using micro-channel plasma targets,” *Physics of Plasmas* **26**, 033110 (2019).
- ⁶S. Zhou, J. Hua, W. An, W. B. Mori, C. Joshi, J. Gao, and W. Lu, “High efficiency uniform wakefield acceleration of a positron beam using stable asymmetric mode in a hollow channel plasma,” *Physical Review Letters* **127** (2021), 10.1103/physrevlett.127.174801.

- ⁷K. Sugimoto, N. Higashi, N. Iwata, A. Sunahara, T. Sano, and Y. Sentoku, “PIC simulation for dense high z plasma formation with ultrashort petawatt laser including radiation processes,” *High Energy Density Physics* **36**, 100816 (2020).
- ⁸E. Adli, A. Ahuja, O. Apsimon et al., “Experimental observation of proton bunch modulation in a plasma at varying plasma densities,” *Physical Review Letters* **122** (2019), 10.1103/physrevlett.122.054802.
- ⁹K. Jiang, A. Pukhov, and C. T. Zhou, “Magnetic field amplification to gigagauss scale via hydrodynamic flows and dynamos driven by femtosecond lasers,” *New Journal of Physics* **23**, 063054 (2021).
- ¹⁰M. Murakami, A. Arefiev, and M. A. Zosa, “Generation of ultrahigh field by micro-bubble implosion,” *Scientific Reports* **8** (2018), 10.1038/s41598-018-25594-3.
- ¹¹M. Murakami, A. Arefiev, M. A. Zosa, J. K. Koga, and Y. Nakamiya, “Relativistic proton emission from ultrahigh-energy-density nanosphere generated by microbubble implosion,” *Physics of Plasmas* **26**, 043112 (2019).
- ¹²J. K. Koga, M. Murakami, A. V. Arefiev, Y. Nakamiya, S. S. Bulanov, and S. V. Bulanov, “Electron-positron pair creation in the electric fields generated by micro-bubble implosions,” *Physics Letters A* **384**, 126854 (2020).
- ¹³S. Fujioka, Z. Zhang, K. Ishihara, K. Shigemori, Y. Hironaka, T. Johzaki, A. Sunahara, N. Yamamoto, H. Nakashima, T. Watanabe, H. Shiraga, H. Nishimura, and H. Azechi, “Kilotesla magnetic field due to a capacitor-coil target driven by high power laser,” *Scientific Reports* **3** (2013), 10.1038/srep01170.
- ¹⁴Y.-J. Gu and S. V. Bulanov, “Magnetic field annihilation and charged particle acceleration in ultra-relativistic laser plasmas,” *High Power Laser Science and Engineering* **9** (2021), 10.1017/hpl.2020.45.
- ¹⁵X. X. Pei, J. Y. Zhong, Y. Sakawa, Z. Zhang, K. Zhang, H. G. Wei, Y. T. Li, Y. F. Li, B. J. Zhu, T. Sano, Y. Hara, S. Kondo, S. Fujioka, G. Y. Liang, F. L. Wang, and G. Zhao, “Magnetic reconnection driven by gekko XII lasers with a helmholtz capacitor-coil target,” *Physics of Plasmas* **23**, 032125 (2016).
- ¹⁶K. F. F. Law, Y. Abe, A. Morace, Y. Arikawa, S. Sakata, S. Lee, K. Matsuo, H. Morita, Y. Ochiai, C. Liu, A. Yogo, K. Okamoto, D. Golovin, M. Ehret, T. Ozaki, M. Nakai, Y. Sentoku, J. J. Santos, E. d'Humières, P. Korneev, and S. Fujioka, “Relativistic magnetic reconnection in laser laboratory for testing an emission mechanism of hard-state black hole

- system,” *Physical Review E* **102** (2020), 10.1103/physreve.102.033202.
- ¹⁷P. Korneev, E. d’Humières, and V. Tikhonchuk, “Gigagauss-scale quasistatic magnetic field generation in a snail-shaped target,” *Physical Review E* **91** (2015), 10.1103/physreve.91.043107.
- ¹⁸P. Korneev, “Magnetized plasma structures in laser-irradiated curved targets,” *Journal of Physics: Conference Series* **788**, 012042 (2017).
- ¹⁹M. Murakami, J. J. Honrubia, K. Weichman, A. V. Arefiev, and S. V. Bulanov, “Generation of megatesla magnetic fields by intense-laser-driven microtube implosions,” *Scientific Reports* **10** (2020), 10.1038/s41598-020-73581-4.
- ²⁰K. Weichman, M. Murakami, A. P. L. Robinson, and A. V. Arefiev, “Sign reversal in magnetic field amplification by relativistic laser-driven microtube implosions,” *Applied Physics Letters* **117**, 244101 (2020).
- ²¹D. Shokov, M. Murakami, and J. Honrubia, “Laser scaling for generation of megatesla magnetic fields by microtube implosions,” *High Power Laser Science and Engineering* , 1–17 (2021).
- ²²K. Weichman, M. Murakami, A. P. L. Robinson, and A. V. Arefiev, “Sign reversal in magnetic field amplification by relativistic laser-driven microtube implosions,” *Applied Physics Letters* **117**, 244101 (2020).
- ²³T. D. Arber, K. Bennett, C. S. Brady, A. Lawrence-Douglas, M. G. Ramsay, N. J. Sircombe, P. Gillies, R. G. Evans, H. Schmitz, A. R. Bell, and C. P. Ridgers, “Contemporary particle-in-cell approach to laser-plasma modelling,” *Plasma Physics and Controlled Fusion* **57**, 1–26 (2015).
- ²⁴D. W. Forslund, J. M. Kindel, and K. Lee, “Theory of hot-electron spectra at high laser intensity,” *Physical Review Letters* **39**, 284–288 (1977).
- ²⁵S. C. Wilks, W. L. Kruer, M. Tabak, and A. B. Langdon, “Absorption of ultra-intense laser pulses,” *Physical Review Letters* **69**, 1383–1386 (1992).
- ²⁶Y.-J. Gu and M. Murakami, “Magnetic field amplification driven by the gyro motion of charged particles,” *Scientific Reports* **11** (2021), 10.1038/s41598-021-02944-2.

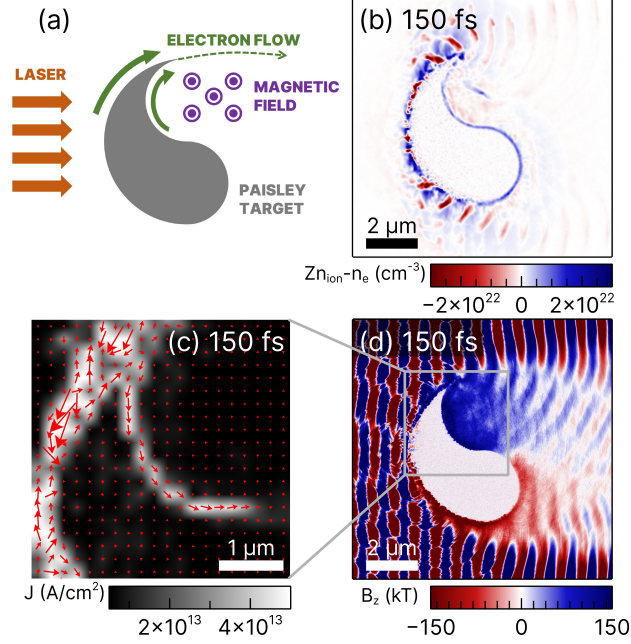


FIG. 1. (a) Illustration of the magnetic field generation mechanism. At $t = 150$ fs, (b) charge separation profile, (c) vector diagram for the net current, and (d) magnetic field profile along the z-axis.

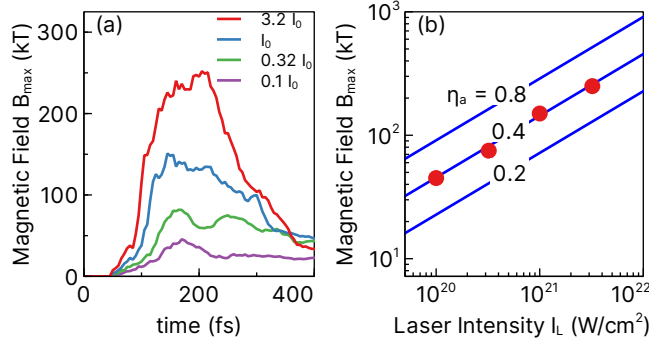


FIG. 2. (a) Maximum magnetic field generated by the paisley target vs time for various laser intensities ($I_0 = 10^{21} \text{ W cm}^{-2}$). (b) Simple analytic model (blue lines) for varying η_a and the maximum magnetic field from the simulations results (red dots).

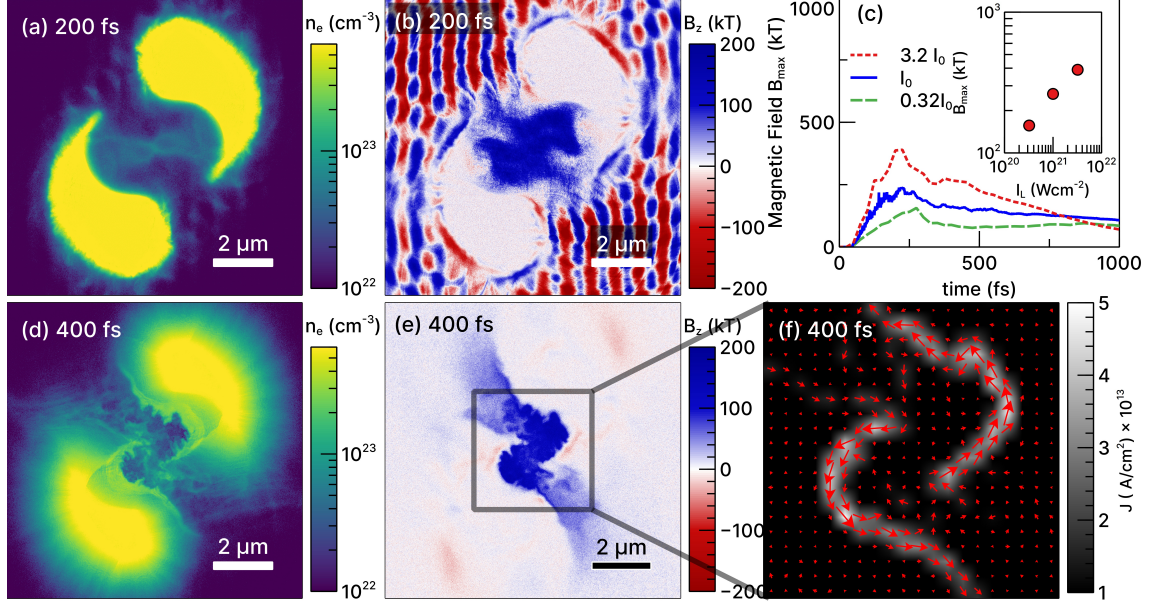


FIG. 3. At $t = 200$ fs, (a) the electron density profile and (b) the magnetic field profile, B_z . (c) Maximum magnetic field as a function of time at different intensities. The inset shows the magnetic field strength as a function of laser intensity. At $t = 400$ fs (d) the electron density profile, (e) the magnetic field profile, and (f) the current vector diagram.

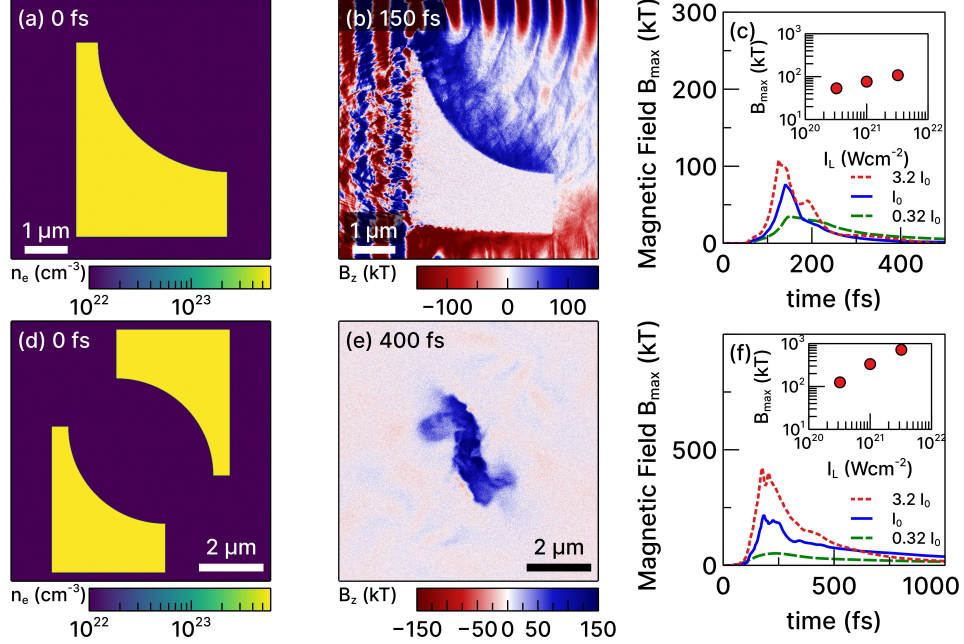


FIG. 4. Simplified single paisley design: (a) Initial electron density profile, (b) magnetic field profile at $t = 150$ fs, and (c) time evolution of the magnetic field strength. Inset shows the magnetic field strength as a function of laser intensity. Simplified double paisley design: (d) Initial electron density profile and (e) magnetic field profile at $t = 400$ fs, and (f) time evolution of the magnetic field strength. Inset shows the magnetic field strength as a function of laser intensity.

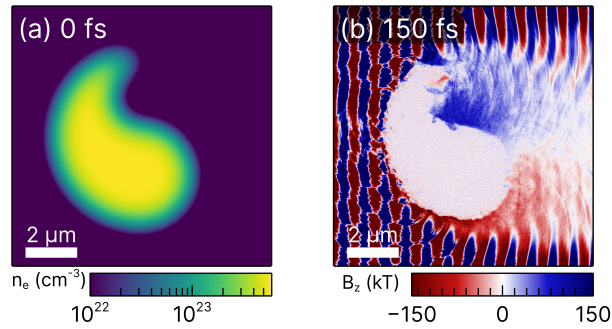


FIG. 5. (a) Initial electron density profile and (b) magnetic field profile at $t = 150$ fs for the pre-expanded case.